SHORT AND LONG-TERM DYNAMICS OF CHILDHOOD DISEASES IN DYNAMIC SMALL-WORLD NETWORKS

J. VERDASCA

Centro de Matemática e Aplicações Fundamentais
Complexo Interdisciplinar da Universidade de Lisboa
Av. Professor Gama Pinto 2, P-1649-003 Lisboa, Portugal[*]

We have performed individual-based lattice simulations of SIR and SEIR dynamics to investigate both the short and long-term dynamics of childhood epidemics. In our model, infection takes place through a combination of local and long-range contacts, in practice generating a dynamic small-world network. Sustained oscillations emerge with a period much larger than the duration of infection. We found that the network topology has a strong impact on the amplitude of oscillations and in the level of persistence. Diseases do not spread very effectively through local contacts. This can be seen by measuring an *effective* transmission rate β_{eff} as well as the basic reproductive rate R_0. These quantities are lower in the small-world network than in an homogeneously mixed population, whereas the average age at infection is higher. **Keywords**: Lattice model; Recurrent epidemics; Small-world networks

1. Introduction

The recurrent outbreaks of measles and other childhood diseases is one of the most striking features of the pre-vaccination records. Despite continuing efforts over more than seven decades, the question of what is the mechanism behind these oscillations has not yet received a fully satisfactory answer [1].

Measles, mumps, varicella (chickenpox) and rubella are examples of diseases that confer lifelong immunity, and can be analyzed within the SIR (Susceptible, Infected and Recovered) or SEIR (comprising an additional class, the Exposed) general frameworks. If the population is constant, the mean-field implementation of SIR and SEIR scheme disregarding heterogeneity in contact structure leads to systems of respectively two and three coupled ODE's. Although based on this most unrealistic description of

---

[*]Present address: Centro de Astrobiologia, Instituto nacional de Técnica Aeroespacial, Ctra. de Torrejón a Ajalvir, km 4, 28850 Torrejón de Ardoz, Madrid, Spain.

2

human contacts, mean-field deterministic models still capture most *static* properties of epidemics of typical childhood diseases including the threshold values for the spread of an epidemic, its final size as well as the average age at which infection is acquired. However, these models fail in that they predict oscillations that are invariably damped. This, of course, contradicts the available records which evidence self-sustained oscillations of roughly constant period during the pre-vaccination era.

After a period during which complicated age-structured models were favored, seasonally forced models have become the framework of choice to explain the historic time-series. In fact, when subject to parametric forcing, deterministic SIR and SEIR ODE's display a rich dynamical behaviour including period-doubling cascades to chaos, quasiperiodicity, multistability between cycles of different periods, etc. [2,3]. When the drive is sinusoidal, the level of forcing at which complex behaviour is observed is deemed unreasonable. However, when a more realistic formulation is used, like an alternating sequence of periods of high and low transmissibility mimicking the opening and closing of schools, the levels of forcing required to obtain complex behaviour is considerably lowered [2,4]. If epidemics correspond to periodic orbits perturbed by noise, as opposed to chaotic solutions [5,6], then only periods which are integer multiples of the forcing period are allowed. More likely, the observation of both integer and non-integer periods in incidence time series of rubella and chickenpox is the signature of an autonomous system oscillating with a frequency that may or may not become locked with an external drive [7].

By definition, there is one important feature that cannot be described by deterministic models. That is the pattern of disease persistence, *i.e.* the probability that a recurrent epidemic goes extinct after a given number of cycles. Persistence is an emergent property arising from the interaction of stochastic effects and dynamics. Its meaningfulness derives from being the key ingredient in the definition of the Critical Community Size (CCS), the population number below which a particular disease cannot be sustained. But persistence is also a tool to assess the relative merits of stochastic versus deterministic models. Indeed, by far the most serious shortcoming of deterministic forcing is that during the minima often the fraction of infective individuals falls below 10^{-10}, meaning that the global human population would not be enough to sustain recurrent epidemics.

It is well known that, like forcing, stochastic effects also tend to sustain the oscillations [8]. However, the implementation of stochastic SIR and SEIR dynamics disregarding heterogeneity in contact structure, generates only

fluctuations which are much too small and irregular when compared to real epidemics unless immigration of infectives from outside is introduced.

Realizing that deterministic forced models fail short of explaining the patterns of persistence and that stochasticity alone could not provide for the necessary agreement with data, researchers began to explore the role of spatial factors in the persistence and dynamics of epidemics. The traditional way to account for an explicit spatial dependence in population ecology and epidemiology is through the use of metapopulation, or patch, models. These are based on a coarse-grained distribution of the global population over a number of interacting subpopulations – the patches. Within-patch dynamics is built into the model *a priory* and can be made as complex as one wishes to from the start, with heterogeneity effects restricted to the coupling between the patches. The coarse-graining procedure limits the ability of the model to assess the impact of the structure of individual contacts on the overall dynamics. It says very little about how emergent complex behaviour on a global scale can arise from simple interaction rules, either strictly local or not. To address this issue one must consider instead a network of interacting individuals.

Nevertheless, some interesting results have been achieved by adding metapopulation structure to stochastic models, either in conjunction with external forcing or not. Lloyd and May [9] simulated a two-patch stochastic SEIR model, each one having at least 10^6 nodes. The oscillations they obtained were too irregular and their amplitude too small when compared with data records.Moreover, strong coherence could not be obtained unless a considerable level of seasonal forcing was applied. However, in that case the number of infective individuals dropped to the unrealistic levels predicted by deterministic models. Bolker and Grenfell [10] considered a similar model but allowed for contacts inside each subpopulation and between individuals belonging to different subpopulations. By increasing the ratio of between- and within-patch contacts they could increase the levels of persistence. Although their study clearly indicated that adding structure to the network of contacts could indeed enhance persistence it greatly overestimated the size of the population needed to sustain recurrent epidemics.

It is interesting to note that the modelling of disease spread as a combination of local and long-range interactions in the context of patch models[10] actually precedes the introduction by Watts and Strogatz of a class of networks that interpolates between regular lattices and random networks [12] – small-world (SW) networks – and the acknowledgment of the importance of the small-world phenomenon on the spread of epidemics that soon followed

4

[13,14,15,16,17]. Subsequently Boots & Sasaki [16] have used SW networks to analyze the selection of a particular strain of a pathogen and Keeling [18] considered a network of nodes which had many of the properties of a SW to calculate epidemic thresholds and determine a number of properties of the endemic state.

More recently, probabilistic cellular automata (PCA) models of infectious diseases evolving on SW networks were proposed by Johansen [19,20], Kuperman and Abramson [21] and He and Stone [22]. These particular models belong to the SIS (Susceptible-Infective-Susceptible) class, that is they apply to diseases which do not confer lifelong immunity. Therefore they are not suited to describe typical childhood diseases. A more problematic feature common to all these studies is that they predict oscillations with periods on the scale of infection and/or immune periods. In contrast, recurrent epidemics of childhood diseases have periods from a dozen up to a few hundred times the infection cycle. Notwithstanding, these models are certainly of great interest as toy models of generic SIS dynamics.

Whether recurrent epidemics are governed by an external drive or by the intrinsic nonlinear dynamics has been the focus of intensive debate practically since the dawn of theoretical epidemiology. Here we make a further contribution to this still unfinished debate by presenting a stochastic model that discards external factors and considers instead the heterogeneity of the contact network. As reported in a previous publication [23] the stochastic implementation of SIR dynamics in a small-world network can describe the onset of epidemic cycles in a population, without considering any exogenous factors such as seasonal forcing or immigration of infectives from outside. In our model, infection takes place through a combination of local rules and long-range contacts, generating a dynamic small-world network. In sharp contrast to the previous studies in the same vein [19,20,21], we observe the emergence of a characteristic time scale which is not that of birth (replenishment of susceptibles) neither is it related in any trivial way to the period of infection.

The results in this paper are arranged in two main parts. The first one is devoted to the SIR implementation. A first set of simulations of long-term behaviour shows that the network topology has a strong impact both on the amplitude of oscillations and the level of persistence. Then, we consider the evolution of an epidemic in a closed population, with birth and death rates set to zero. We show that the basic reproductive rate, R_0, increases from its minimum value in a regular lattice with local contacts only up to the maximum, mean-field value, as the percentage of long-range infection

is increased from zero to one. In the second part of the paper we present simulations of the more realistic SEIR version. We calculate the period and amplitude of oscillations, R_0, as well as the average age at infection for realistic demographic and etiological parameters corresponding to measles, rubella and chickenpox.

The detailed structure of the paper is the following: in Section 2 we describe the algorithm in detail; in Section 3 we present the results of the SIR model and in Section 4 those of the SEIR model. This is followed by a Discussion and, finally, the Conclusion.

2. PCA Model

2.1. *General description*

Here we describe the probabilistic cellular automata (PCA) implementation of the SIR model that has been briefly outlined in a preceding paper [23].

Individuals live on a square lattice of $N = L \times L$ sites. The bonds between sites are connections along which the infection may spread to other individuals. Infection proceeds either locally, within a prescribed neighbourhood, or through a link established at random between any two individuals. We introduce a small-world parameter p_{SW} defined as the fraction of attempts at infection carried out through a random link; $p_{\text{SW}} = 0$ corresponds to a regular lattice where each individual contacts with his k nearest neighbours only, while $p_{\text{SW}} = 1$ corresponds to a random network. For intermediate values of p_{SW} the network of contacts is neither fully ordered nor completely random.

2.2. *Algorithm*

We choose first between *birth*, *death* and *infection* events, the latter being either *local* or *long-range* with respective probabilities $p_{\text{inf}}^{loc} = (1 - p_{\text{SW}})\beta_0$ and $p_{\text{inf}}^{lr} = p_{\text{SW}}\beta_0$. (Note that we call long-range link any connection established at random to any node on the lattice, not only those that connect to sites lying outside the established neighbourhood). The total population number if fixed, therefore $p_{birth} \equiv p_{death}$. $\beta_0 = p_{\text{inf}}^{loc} + p_{\text{inf}}^{lr}$ is the total probability of an attempt at infection while $(1 - p_{birth} - p_{death} - p_{\text{inf}}^{loc} - p_{\text{inf}}^{lr})$ is the probability that nothing happens. There is no restriction associated to the fact that the sum of probabilities cannot exceed one because it is possible to attribute any weight to any one of the events - birth, death or infection - by a suitable choice of the time scale; the probability of

6

not realizing any event will change accordingly and a sweep through the lattice will simply correspond to a different time unit. In one time unit, or PCA step, we perform N attempts to realize one given event, as follows: we generate a random number r uniformly distributed between 0 and 1. If $0 < r \leq p_{birth}$ we make an attempt to realize a birth event; if $p_{birth} < r \leq p_{birth} + p_{death}$ an individual picked at random will die; if $p_{birth} + p_{death} < r \leq p_{birth} + p_{death} + p_{\inf}^{loc}$ an attempt at local infection is made while if $p_{birth} + p_{death} + p_{\inf}^{loc} < r \leq p_{birth} + p_{death} + p_{\inf}^{loc} + p_{\inf}^{lr}$ the attempt will be long-ranged. Finally, if $p_{birth} + p_{death} + p_{\inf}^{loc} + p_{\inf}^{lr} < r \leq 1$, we just carry on and generate a new random number. The realization of the events is the following:

(1) Attempt at local infection or long-range infection: First choose a site i at random; Then,

    (a) If that site is occupied by a recovered (R) individual or an infectious (I) individual, do nothing.

    (b) If it is occupied by a susceptible (S) then choose another site j from a list of k possible neighbours, in the case of local infection, or from all of the N sites, with equal probability, in the case of long-range infection. In the simulations presented here, the local range comprises nearest neighbours, next nearest neighbour and third nearest neighbours ($k = 12$). If,

      i. Site j is occupied either by another susceptible or a recovered individual: do nothing.

      ii. The site is occupied by an infective: The first individual becomes infected.

(2) A death event is chosen. Then one picks an individual at random who dies irrespectively of his present state. The probabilities of death are then proportional to the density of S, I and R individuals. Susceptible and infective individuals who die become recovered; recovered individuals remain in that same class.

(3) Birth event: one looks at the lattice (at random) for a recovered individual. Once found, that individual becomes susceptible. The trial only ends when one actually finds a recovered individual, so that the birth rate, as it should, is independent of any density.

After a time during which he stays infectious to others, the individual recovers. He becomes immune for life and cannot be infected again. For childhood diseases these periods vary only by a small amount among indi-

viduals within a population. So, it is more realistic to assume a constant infectious period - deterministic recovery - than a constant probability of recovery leading to an exponential distribution of infectious periods [24]. We model deterministic recovery by associating a counter n_r to every individual. Upon infection, the counter for that individual is updated at each time step, $n_r \rightarrow n_r + 1$. At each PCA step we move to the recovered class those infectives for which the counter has reached the fixed infectious period τ, and reset their counter. Stochastic recovery, on the other hand, is modelled by a Poisson process: we add a new event to the list above – a recovery event – taking place with probability γ. When such event is chosen, one picks an individual at random; if infective, that individual is moved into the recovered class, otherwise nothing happens.

The SEIR model comprises one additional class, the exposed (E). After being infected, the individuals enter a latency period during which they cannot be re-infected yet they are unable to transmit the infection to others. In our simulations the individuals move deterministically from the exposed to the infectious class after τ_{lat} steps and then stay infectious for τ_{inf}.

One important difference between the model and the population dynamics in developed countries is the implicit assumption of the so-called Type II mortality, where individuals die with equal probability independently of their age, as opposed to Type I mortality where all individuals live up to the same age and then die [1].

3. Results: SIR model

3.1. *Persistence*

Recurrent epidemics can persist in finite populations because of the finite birth rate that allows for the renewal of susceptibles. The way in which persistence varies with the small-world parameter p_{SW} depends crucially on the rate at which fresh susceptibles are supplied by birth. As shown in Fig. 1, for intermediate values of μ the persistence coefficient is zero at low p_{SW}, and approaches one over a narrow range of p_{SW}. At values $\mu \lesssim 0.001$ a maximum starts to develop. Barely noticeable at $\mu = 0.0006$, it is already quite pronounced at $\mu = 0.0004$. At $p_{SW} = 1.0$, only about half the runs survive up to the maximum ascribed time, whereas within the range $p_{SW} = 0.2 - 0.3$ more than 90 % of the runs reach t_{max}. The relevant fact is that at low enough birth rates there is an optimal value of p_{SW} for the disease to persist in finite populations. Conversely, for $\mu \gtrsim 0.001$ the persistence coefficient shows a minimum at finite p_{SW}. The logarithmic scale in Fig. 1
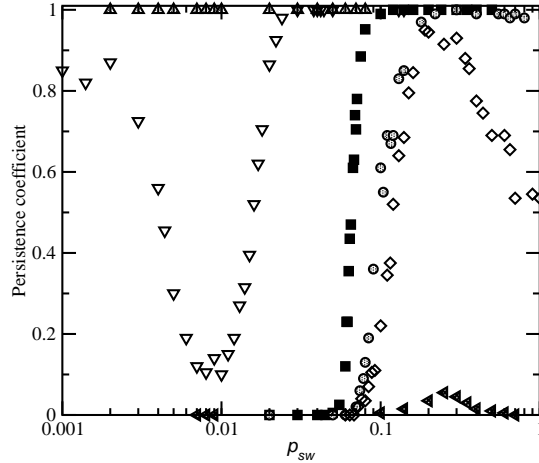
8

Figure 1.   Persistence coefficient, defined as the fraction of runs that attain a
prescribed time $t_{max} = 20000$ of a total of $n = 100$ runs started, calculated on a
400×400 lattice with deterministic recovery. The initial fraction of susceptibles
was $s_0 = 0.165$. The probability of infection is $\beta_0 = 0.66$ and the infectious period
$\tau = 16$. The different curves correspond to the following birth rates: $\mu = 0.0002$
(triangles left), $\mu = 0.0004$ (diamonds), $\mu = 0.0006$ (circles), $\mu = 0.001$ (squares),
$\mu = 0.002$ (triangles down) and $\mu = 0.005$ (triangles up).

enables us to highlight this remarkable symmetry of behaviour but here we
must note that what happens at high birth rates is irrelevant for childhood
diseases. Indeed, for τ given in days (which is not unreasonable) we get a
birth rate of $\mu = 0.002$ day^{-1} corresponding to an average lifespan of 1.4
years! Even for the lowest μ with which we can still observe a reasonable
level of persistence, the lifespan would only be around 7 years. This feature
is a distinguishing property of the PCA implementation of the SIR model,
namely that to obtain realistic patterns of persistence one has to choose
birth rates at least one order of magnitude higher than the real values. We
shall see in Section 4, that the adoption of the more realistic SEIR dynamics
permits to avoid this problem.

The fact that persistence depends on the fraction of long-range con-
tacts implies that the Critical Community Size (CCS) also depends on the
structure of the contact network. In order to demonstrate how the PCA
can be used to estimate the Critical Community Size, and how the CCS
depends on the fraction of long-range infection we choose two examples, at
$p_{\text{SW}} = 0.07$ and $p_{\text{SW}} = 0.1$, with a birth rate $\mu = 0.001$ (squares in Fig.

1). While at $p_{\text{SW}} = 0.1$ there is a sharp rise in persistence, at $p_{\text{SW}} = 0.07$ a much smoother curve is obtained (Fig. 2). The population size at which the persistence rises above 50 % can be taken as a estimate of the CCS but we might as well choose a different threshold.
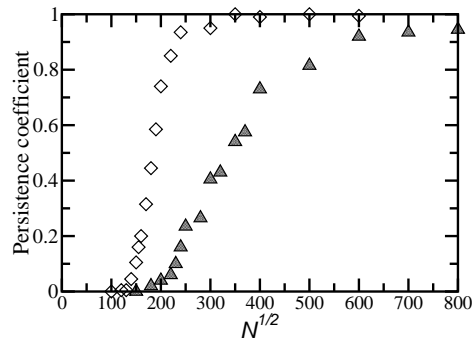

Figure 2. Persistence coefficient as a function of lattice size for $p_{\text{SW}} = 0.07$ (triangles) and $p_{\text{SW}} = 0.1$ (diamonds) at $\mu = 0.001$. The other parameters are the same as in Fig. 1 except $n = 200$.

3.2. *Amplitude of oscillations*

Fig. 3 shows a typical output of the SIR model implemented on a fairly large lattice. The time series shown are for the susceptible and infective fraction. It is impossible to run the three-state SIR implementation for a long time using realistic demographic and etiological parameters. Extinction is almost certain to occur after only a few cycles. Thus the values of the birth rates used here are much larger that real ones, again for a τ of a few days.

When p_{SW} is small, the oscillations have large amplitudes and are strongly synchronized. Keeping all other parameters unchanged but setting $p_{\text{SW}} = 1.0$ we observe that oscillations become much more irregular and their amplitude is considerably diminished. In Fig. 4 we plot the root mean square (RMS) amplitude of the oscillations in the fraction of susceptibles (a) and infectives (b) as a function of the birth rate for different values of p_{SW}. As μ is decreased the RMS amplitudes are amplified and this trend is the more pronounced the smaller the value of p_{SW}.

Looking at the data from a different perspective now, one detects quite clearly the enhancement of stochastic fluctuations growing into fully developed oscillations as the relative weight of long-range infection is decreased.
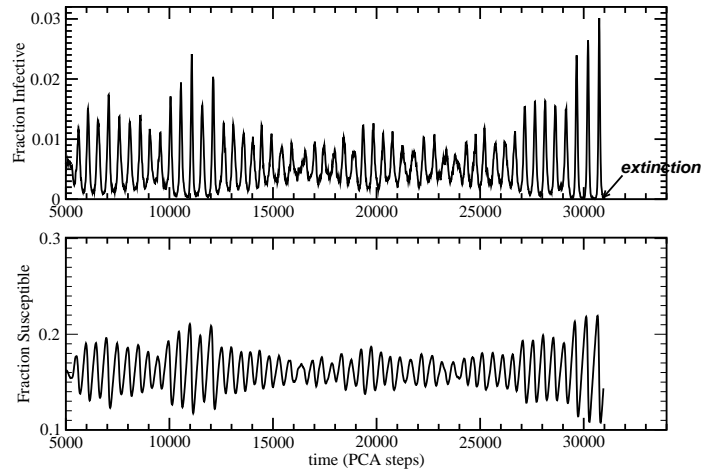
Figure 3.   Typical evolution of the fraction of infectives (top) – number of infective individuals divided by the system size N – and the fraction of susceptibles (bottom), obtained with the SIR PCA model implemented on a small-world network of $N = 160000 \equiv 400 \times 400$ individuals. In the simulations, 90 % of the contacts are local and the remaining 10 % long-range ($p_{\mathrm{SW}} = 0.1$). Recovery was stochastic with a probability $\gamma = 0.0625 \equiv 1/16$. The other parameters are $\mu = 0.0004$ and $\beta_0 = 0.66$. The system oscillates for more than 50 cycles before extinction occurs after about 30950 PCA steps.

The smaller the birth rate the more accentuated the effect becomes: at $\mu = 0.001$ the amplitude of the susceptible oscillations at $p_{\mathrm{SW}} = 0.08$ is approximatively four times that of the homogeneous mixed population while at $\mu = 0.0004$ the same ratio is almost five. The increase in the amplitude of oscillations in the fraction of infectives (Fig. 4 (b)) follows that of susceptibles but it is less marked.

3.3. *Effective transmission rate*

Diseases do not spread very effectively on lattices when only local contacts are allowed because infective individuals tend to interact mostly with other already infected individuals. To evaluate the impact of the aggregation of infectives and susceptibles into clusters on the spread of the disease brought about by the local contact rules we can estimate the transmission rate directly from the simulations. This is done by observing that once the transients have died out, the mean number of new infections that take place in a short time interval Δt, $nni_{\Delta t}$, is approximatively proportional to the
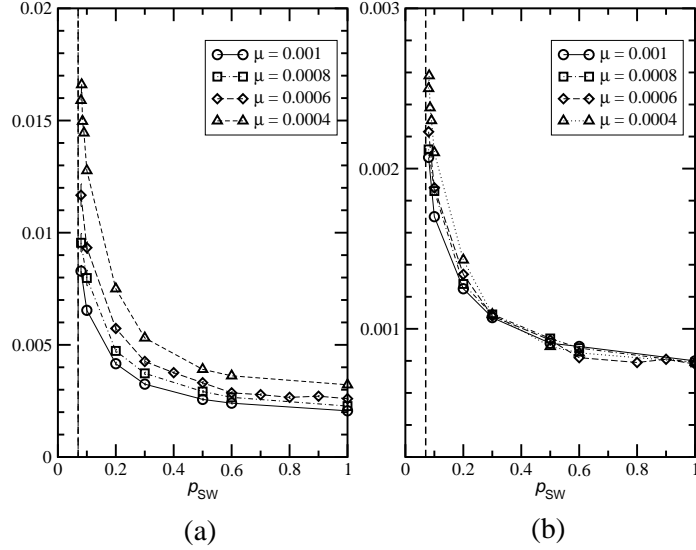
Figure 4.   RMS amplitude of oscillations in the fraction of susceptibles (a) and infectives (b) as a function of the fraction of long-range contacts for decreasing values of the birth rate. Other parameters the same as in Fig. 3. Stochastic recovery. Each point represents an average over 10 runs started from different initial conditions.

product of the mean number of infective individuals by the mean number of susceptibles during that same time interval:

$$nni_{\Delta t} \sim \overline{I}_{\Delta t} \times \overline{S}_{\Delta t}. \tag{1}$$

The sensitive issue here is to choose a suitable value for Δt, which must be much smaller than the average period of oscillations or otherwise we would not get an instantaneous measure of transmission, but at the same time considerably larger than the infection period so that stochastic effects get averaged out. There is no recipe to pick up the right value, but choosing a Δt of a few dozen time steps usually guarantees that the proportionality (1) is verified. In that case, we can define an *effective* transmission rate as:

$$\beta_{\text{eff}}(t) = \frac{nni_{\Delta t}(t)}{\overline{I}_{\Delta t}(t)\overline{S}_{\Delta t}(t)}. \tag{2}$$

This instantaneous transmission rate fluctuates wildly on the time scale of the birth rate but once the transients have died out we can calculate the temporal mean. This (averaged) effective transmission rate stays always below the mean-field transmissibility β_0. Indeed, by aggregating infectives

12

and susceptibles into clusters, the structure of local infection on a *regular* network structure acts to keep the number of contacts that can actually result in transmission, namely those between a susceptible and an infective, well below the level that would result if the individuals were homogeneously distributed on the lattice irrespectively of their disease status. Although, as we shall see below, the dynamic small-world structure of contacts exhibits some features of the well-mixed situation, *locally* the structure of contacts remains highly clustered. As long as infected individuals remain in contact mostly with other already infected individuals the progression of the disease stalls but once an individual belonging to an infectious cluster establishes a shortcut that propagates the disease into a region where susceptible individuals predominate, the disease will perhaps get a new boost that will carry it through one more cycle.
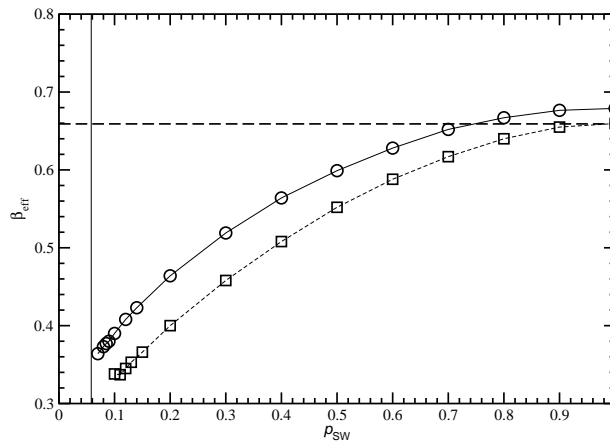

Figure 5.   Effective transmission rate β_{eff} vs. the small-world parameter p_{SW}. The reduction of β_{eff} that arises both for deterministic (circles) and stochastic (squares) recovery is due to the clustering of infectives and susceptibles. The dashed line indicates the value of the transmissibility, or total probability of realizing an infection event used in the simulations: $\beta_0 = 0.66$. Note the almost perfect agreement with the mean-field result $\beta_{\text{eff}} \equiv \beta_0$ observed at $p_{\text{SW}} = 1.0$ for stochastic recovery. The birth rate is $\mu = 0.0006$, the infectious period for deterministic recovery $\tau = 16$ and $\gamma = 0.0625 \equiv 1/\tau$ for stochastic recovery. Each point represents an average over 10 runs.

As shown in Fig. 5, β_{eff} increases smoothly as p_{SW} increases. For values of p_{SW} to the left of the lower end of the curves only a very small fraction

of the runs last for more than a few cycles. With such a small persistence it becomes impossible to follow the long term dynamical regime and compute repeated time averages of non-transient oscillations. The two curves shown in Fig. 5 correspond to stochastic and deterministic recovery. Their shape is identical, but the value of β_{eff} for stochastic recovery always stays below that obtained with deterministic recovery. The values of β_{eff} for stochastic recovery converge to the mean-field value for $p_{\text{SW}} \to 1$ with a small discrepancy due to finite-size effects, whereas for deterministic recovery β_{eff} is still about 3 % above β_0 in the same limit. Moreover we found that the amplitude of oscillations is also larger for deterministic recovery than for stochastic recovery, the differences being small at large p_{SW} but increasing significantly as p_{SW} is lowered. This is in agreement with a previous study of a homogeneously mixed stochastic model, showing that sharp distributions of the infection period result in larger fluctuations than those with a smooth distribution [24]. In our model this effect actually intensifies when contact structure is introduced.

3.4. *Basic reproductive rate*

It is incontrovertibly accepted that in order to figure out if a given pathogen will be able to succeed in a host population the crucial quantity to compute is the basic reproductive rate R_0. This is the number of secondary infections produced by an infected individual in a population entirely composed of susceptibles.

The analysis of steady state solution of the SIR deterministic ODE's considering only weak homogeneous mixing – meaning that the rate of new infectives is proportional to the total number of susceptibles – and Type II survival, gives [1]:

$$R_0 = \frac{1}{\mu A}, \tag{3}$$

where A is the average age at infection, in the case of constant population size. Under the more stringent condition imposed by the mean-field approximation, one has also [1]

$$R_0 = \frac{\beta N}{\gamma + \mu}. \tag{4}$$

Note that relations (3) and (4) suppose stochastic recovery.

The definition of R_0 rests on the existence of a pristine susceptible population, *i.e.* it is valid only at vanishing infective fraction. However, it

14

is a consequence of mean-field models and a fact confirmed by the analysis of many real epidemics, that following the introduction of a pathogen in a population consisting entirely of susceptible individuals the number of infective individuals grows exponentially in the early stages:

$$I(t) \sim e^{\Lambda t}, \tag{5}$$

where $\Lambda = (R_0 - 1)/\tau$. So, with the exception of incipient epidemics ($R_0 \rightarrow 1$), very soon after an epidemic has started from a single infective, the number of infectives is already too large for the definition of R_0 to apply. What can be measured directly from the PCA in long-time simulations, and in most field studies is rather R_t, the effective reproductive rate at a given time t during the evolution of the disease when there are also infective and recovered individuals present. Upon the further assumption of weak homogeneous mixing, we can write

$$R_{t \rightarrow \infty} = R_0 s^* \tag{6}$$

where s^* is the fraction of susceptibles in the endemic steady-state. If the rate at which susceptible individuals are infected is exactly balanced by the rate at which new susceptibles are born then $\bar{R}_{t \rightarrow \infty} = 1$, where the bar denotes the temporal mean. That is, each primary infection will produce on average exactly one secondary infection. Under these precise conditions, the basic reproductive rate is simply $R_0 = 1/s^*$.

The depletion of susceptibles during the epidemic implies that $R_t < R_0$ always. If R_t is maintained below 1 for sufficiently long, then the pathogen will become extinct. However, as we can see in Fig. 6, R_t calculated directly from the PCA oscillates around an average value which, within statistical errors, is exactly one. R_t drops below the self-sustained threshold for half the period of oscillations only to rise again above it in the next half-cycle. This result has drastic implications on the assessment of the risk of recurrent outbreaks of infectious diseases based on calculations of R_t. It is usually assumed that as soon as R_t drops below 1, an epidemic is on its way to be contained. Very recently this criterium was used to judge the outcome of the SARS epidemic [25,26] based on data spanning only a few weeks. In this vein, the results in Fig. 6 should act as a warning particularly when, as it is often happens, one has to deal with short time series or otherwise incomplete data.

Now we must make the distinction between the long-time measurements, using time averages over (extended) time series of recurrent epidemics and short-time measurements of R_0. For the long-term measurements we have
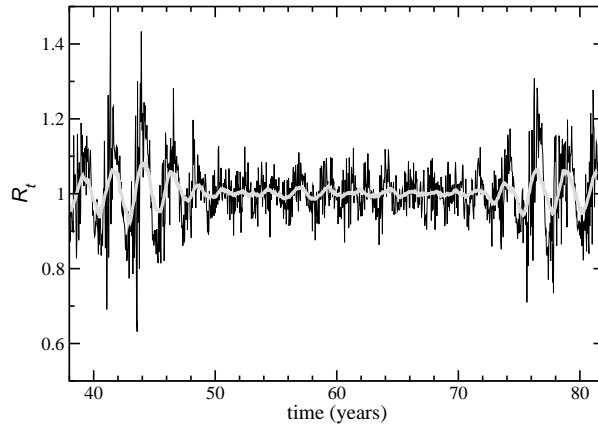
Figure 6.   Evolution of the effective reproductive rate in a SEIR simulation. R_t is calculated by counting the number of secondary infections caused by every infective individuals and taking averages. The result is a very noisy time series which nevertheless shows an underlying structure composed of cycles with the same period as the oscillations in incidence. Smoothing the data by averaging it out with a moving window brings forward the pattern of oscillations (thick plain curve). In the SIR model we observe the same effect only the data contains a lot more noise.

different possibilities to estimate R_0: We can either i) compute A directly from the PCA by the method described in the next Section and then use Eq. 3 to evaluate R_0. ii) Estimate the effective transmissibility β_{eff} as described in Section 3.3 and then compute R_0 from (4) with $\beta \equiv \beta_{\text{eff}}$ or iii) use the fact that $R_t = 1$ once an asymptotic regime is attained and estimate $R_0 = 1/s^*$.

As an alternative to perform lengthy simulations of recurrent epidemics for the purpose of computing R_0, we can run the PCA in a closed population. Discarding births and deaths by setting $\mu = 0$, we can iv) compute the R_0 from the final size equation (FSE) [27]

$$\ln(s_\infty) = R_0(s_\infty - 1) + \ln(s_0), \tag{7}$$

where $s_\infty = S_\infty/N$, with S_∞ the number of susceptibles left once the epidemic has died out. The initial fraction of susceptibles is $s_0 = (N-1)/N$ since every new run begins with a single infective. The last form of computing R_0 that we considered was to v) fit the exponential growth law, Eq. (5), to the early stages of evolution of an epidemic ravaging a wholly susceptible population. The results are presented in Fig. 7. They show how R_0 can be

16

used to assess the departure from mean-field behaviour as the fraction of long-range infection is decreased, and also that in a structured population with the characteristics of a dynamic small-world, the magnitude of R_0 is always below the value that would be obtained in an homogeneously mixed population. Different procedures of estimating R_0 that would give the same result under the mean-filed approximation will now yield markedly distinct values. This is because they still appeal to an approximation at some stage but not all at the same stage. Undoubtedly, this is a blow to the worth of R_0 evaluated in practical situations. Indeed, with the exception of contact tracing in the very early stages of an epidemic, which is a very difficult task to perform, R_0 can only be determined through indirect methods. Our simulations show that evaluating R_0 from different sources, for instance from A obtained from serological studies, or from the equilibrium number of susceptibles obtained from historic time series can lead to *intrinsically* different results as a consequence of the heterogeneity of contacts.

3.5. *Average Age at Infection*

The moment of their lives when susceptible individuals acquire infection is a very important epidemiological quantity. The average age at infection, A is inferred from serological surveys and can be compared to the output of epidemiological models.

We evaluate the impact of network structure on A by calculating it directly from the simulations as follows: a counter is associated to every susceptible and the moment when this individual is infected is recorded. Averaging over every single individual who has become infected so far one obtains a quantity that shows a slow but unremitting trend towards asymptotic behaviour characterized by small, rapid fluctuations around a steady-state value. Once the long term evolution appears to stabilize we compute the time average.

The average age at infection was found to be linear in $1/\mu$ down to only 8 % of long-range contacts. Below that value of p_{SW} persistence was too low to obtain meaningful averages. The slope of the lines in Fig. 8 gives $1/R_0$. Moreover, the ratio $r = R_t A\mu/s^*$ varies from 0.9999 ± 0.0002 at $p_{\mathrm{SW}} = 1.0$ to $r = 0.9994 \pm 0.0001$ at $p_{\mathrm{SW}} = 0.08$ showing that mean-field relations hold to an excellent approximation down to surprisingly low values of p_{SW}. Deviations to mean-field behaviour do occur but are only slight even in relatively small populations. From the data in Fig. 8 we can extrapolate the average age at infection at low birth rates. Setting the time scale by
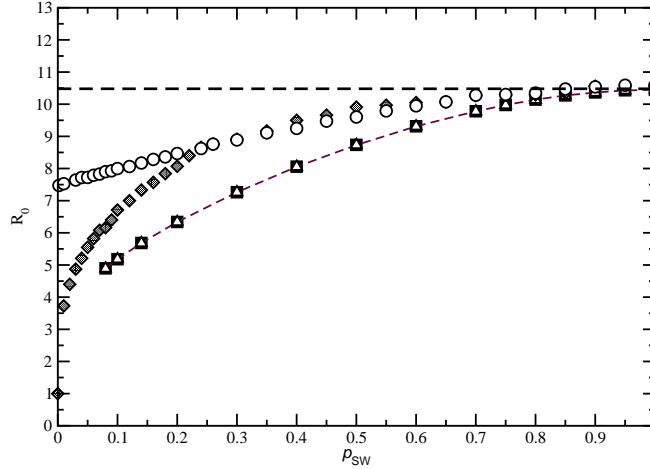
Figure 7. R_0 as a function of the small-world parameter p_{SW}. The two upper curves were calculated from simulations in a closed population ($\mu = 0$), from the final size equation (7) (circles) and by fitting exponential growth using Eq. (5) (diamonds). At p_{SW} the number of infectives grows in time as a power law and therefore $\Lambda \equiv 0$ implying $R_0 \equiv 1$. The curves obtained from the analysis of long-term dynamics using $R_0 = 1/s^*$ (squares) and from A and Eq. (3) (triangles) are almost indistinguishable. In the limit of a random network the four curves converge to $\beta_0/(\gamma + \mu)$, indicated by the dashed line, with a small discrepancy attributed to final size effects. SIR model in a 400×400 lattice with stochastic recovery; parameters are the same as in Fig. 5.

taking $L \equiv 1/\mu = 61$ years we obtain $A = 6$ years for $p_{\mathrm{SW}} = 1.0$, $A = 7.7$ years for $p_{\mathrm{SW}} = 0.3$ and $A = 10.2$ years for $p_{\mathrm{SW}} = 0.08$ showing that the average age at infection increases significantly when we consider a local, clustered network of contacts.

4. Results: SEIR model

4.1. *Epidemic cycles*

We now present numerical simulations of the more sophisticated SEIR model, with etiological and demographic parameters corresponding to measles, rubella and chickenpox, in developed countries, in the pre-vaccination era. Just as in the SIR case we observe sustained oscillations in incidence. The oscillations obtained from the SEIR model are less coherent than those obtained with the SIR version. Their aspect is actually closer to the observed time series.
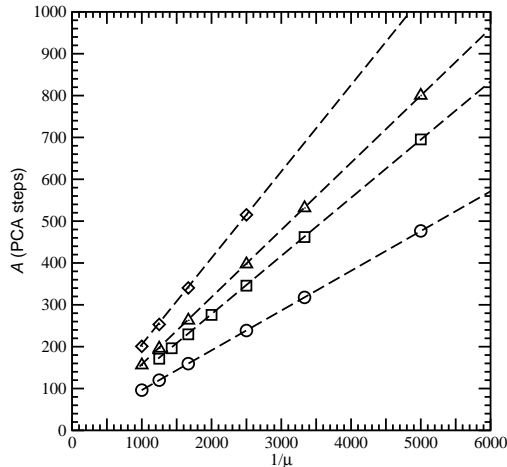
18

Figure 8. The average age at infection measured in PCA steps as a function of life expectancy $1/\mu$ in the same units, for $p_{SW} = 1.0$ (circles), 0.3 (squares), 0.2 (triangles) and 0.08 (diamonds). The slope of the lines gives $1/R_0$. The parameters are $\beta_0 = 0.66$, $\gamma = 0.0625$; the initial infective fraction was $s_0 = 0.165$ and 50 infectives were present on the lattice. The values of A were obtained from a temporal average of data sampled from $t = 10000$ to $t = 50000$ at 10 steps interval and further averaging over 10 realizations starting from different initial conditions.

But the most consequential finding of the SEIR simulations is the realization that one can only obtain sustained oscillations with amplitudes compatible with the existing data records, and for realistic values of the model parameters – (*e.g.* life expectancy, latency and infectious periods) – if one chooses values of p_{SW} in the small-world region [13].

To illustrate this feature, we show in Fig. 9 two time series for measles, one obtained for $p_{SW} = 0.2$ and the other for $p_{SW} = 1.0$. The amplitude of the oscillations is almost double in the small-world network.

For $p_{SW} = 1.0$ the frequency distribution is peaked around 1.5 years while for $p_{SW} = 0.2$ the peak is at about 2.5 years. For measles, almost every data record in developed countries points to cycles of almost exactly 2 years, in between those two values. Agreement with the observed periods can be improved, but only to some extent, by fine tuning the transmissibility. Indeed, increasing β_0 has the effect of decreasing the period making it more in line with the observations. The resulting time series are shown in Fig. 10. Nevertheless, we must stress that β_0 is nothing like a free parameter. First of all it cannot be changed at will in order to tune the
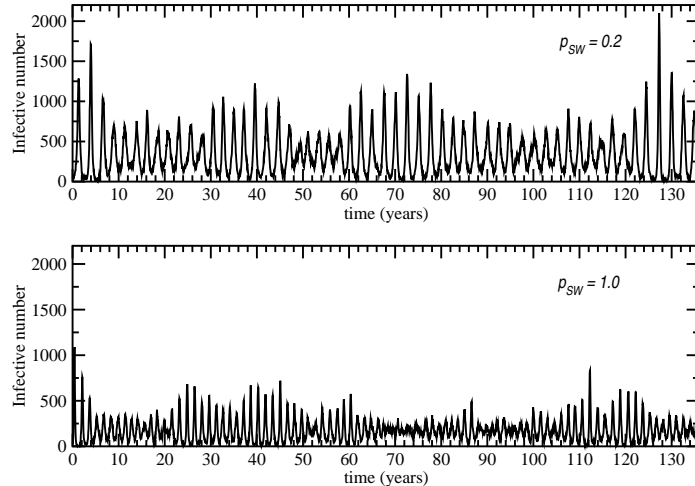
Figure 9.   Time series of the number of infectives obtained from simulations of SEIR dynamics in a 1000×1000 lattice with $\mu = 1/61$ yr^{-1}, $\tau_{lat} = 6$ days, $\tau_{inf} = 8$ days and $\beta_0 = 3.92$ day^{-1}.

period because the amplitude of oscillations also changes and the average size of outbursts must remain comparable to those observed in cities with the same population size [23]. Secondly, since the transmissibility of typical childhood diseases must be similar (see Section 4.3 below), differences in period, average age at infection, etc. between them must be achievable with values of β_0 of the same order of magnitude and respecting the expected infectious rank of those diseases. Finally, and most importantly, although β_0 is a parameter that can only be very loosely inferred from the data, there are indirect estimates of β_{eff} from R_0 and A, using mean-field relations, that set an order of magnitude for β_0.

4.2. *Estimates of A and R_0*

We have computed the average age at infection obtaining $A = 1.6$ years for $p_{\text{SW}} = 1.0$ and 3.6 years for $p_{\text{SW}} = 0.2$ for the simulations shown in Fig. 10, and $A = 1.9$ years for $p_{\text{SW}} = 1.0$, and 4.1 years for $p_{\text{SW}} = 0.2$ for the simulations in Fig. 9. While the latter is just barely above the lower bound of the interval commonly accepted to correspond to measles data – between 4 to 6 years – the values obtained with the homogeneous mixed population lie notably outside the realistic range. A further refinement consisting in the inclusion of protection by maternal antibodies in newborns
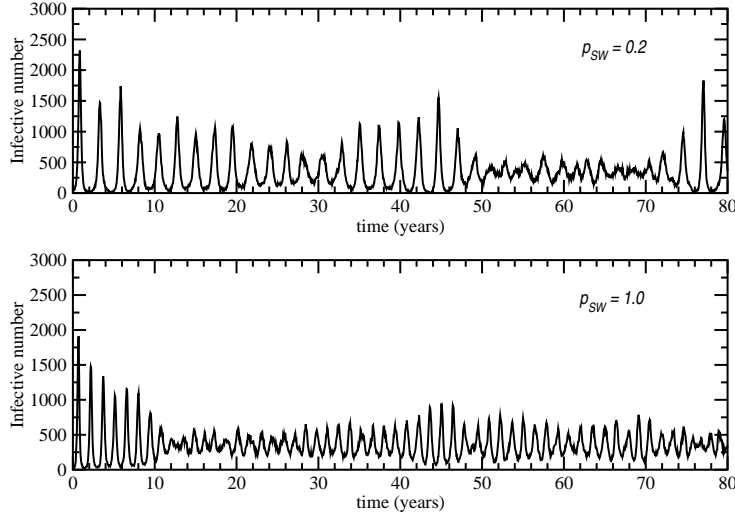
Figure 10.   Same parameters as in Fig. 9 except that now $\beta_0 = 4.75$ day^{-1}. The period of oscillations shrinks when β_0 increases. Note the change of scale in both axes with respect to Fig. 9.

could increase both values by 3 to 9 months putting the result for $p_{SW} = 0.2$ well inside the interval of realistic values. However, this is expected to have a deleterious repercussion on the period of oscillations, increasing it above what is consistent with data records for measles.

For the simulation at $p_{SW} = 0.2$ in Fig. 9, the average fraction of susceptibles was $s^* = 0.0657$ giving a value for $R_0 = 1/s^*$ of 15.2 while for $p_{SW} = 1.0$ we get $s^* = 0.0312$ yielding $R_0 = 32.1$. Whereas the former lies inside the reported range of R_0 for measles, $14 - 18$ [1], the latter is way off range. For the SEIR model, the mean-field expression for R_0 is slightly more complicated than in the SIR case [1]:

$$R_0 = \frac{\beta}{\tau_{inf}^{-1} + \mu} \left(\frac{\tau_{lat}^{-1}}{\tau_{lat}^{-1} + \mu} \right). \qquad (8)$$

Solving for β and using the values of R_0 calculated above we obtain $\beta = 4.0$ and $\beta = 1.9$ for $p_{SW} = 1.0$ and 0.2 respectively. While the former is close to the β_0 used in the simulations, the latter is practically one half. The reason for this is that the transmission rate computed from Eq. (8) is rather the β_{eff} introduced in Section 3.3, and only in the mean-field case do we have $\beta_{\text{eff}} \equiv \beta_0$. The effective transmission rates obtained directly from the simulations by the method of Section 3.3 were $\beta_{\text{eff}} = 1.86$ for $p_{SW} = 0.2$

and $\beta_{\text{eff}} = 3.93$ in the homogeneous mixed case, in very good agreement with the respective β's calculated from Eq. (8).

4.3. *Comparison between childhood diseases*

In this section we show that the ability of the PCA to describe sustained oscillations is not restricted to measles but extends to other childhood diseases conferring life-long immunity. In Figs. 11 and 12 we show long-term runs for etiological parameters corresponding to rubella and chickenpox, respectively. We kept the small-world parameter fixed at $p_{\text{SW}} = 0.2$, since childhood diseases must share a common contact structure. The PCA is nevertheless capable of discriminating between these different diseases, in terms of period, average age at infection and basic reproductive rate.

The periods estimated from the Fourier transform of the time series in Figs. 11 and 12 were $T \approx 4.4$ years for rubella and $T \approx 3.4$ for chickenpox; the average age at infection was $A \approx 6.2$ for rubella and $A \approx 4.7$ for chickenpox. Like for measles, A is considerably underestimated by the PCA, most studies in developed countries giving a lower bound for A of about 9 years for rubella and 6 years for chickenpox. Still, the relative values of A for the three diseases agree with the data [1]. The basic reproductive rate computed from the inverse fraction of susceptibles is about 10 for rubella and 13 for chickenpox. The simulations for measles gave $R_0 \approx 15$. Again, the values for measles and chickenpox are very good while the reproductive rate of rubella is above that reported.

Based on a purely qualitative evaluation of the mode of transmission we can rank common childhood diseases in roughly two classes of infectiousness. Measles and chickenpox are transmitted through aerosol droplets and therefore the most infectious. In the second group we have mumps and rubella which require direct contact with droplets generated by sneezing and coughing. In our simulations, this hierarchy of infectiousness was strictly respected, with $\beta_0^{\text{measles}} > \beta_0^{\text{chickenpox}} > \beta_0^{\text{rubella}}$. The numerical values used in the simulations give a quantitative estimate of infectiousness:

$$\frac{\beta_0^{\text{measles}}}{\beta_0^{\text{rubella}}} = 3.7, \quad \frac{\beta_0^{\text{measles}}}{\beta_0^{\text{chickenpox}}} = 1.9,$$

and the respective effective transmission rates obtained for a fraction of 20 % of long-range contacts give:

$$\frac{\beta_{\text{eff}}^{\text{measles}}}{\beta_{\text{eff}}^{\text{rubella}}} = 2.5, \quad \frac{\beta_{\text{eff}}^{\text{measles}}}{\beta_{\text{eff}}^{\text{chickenpox}}} = 1.7.$$
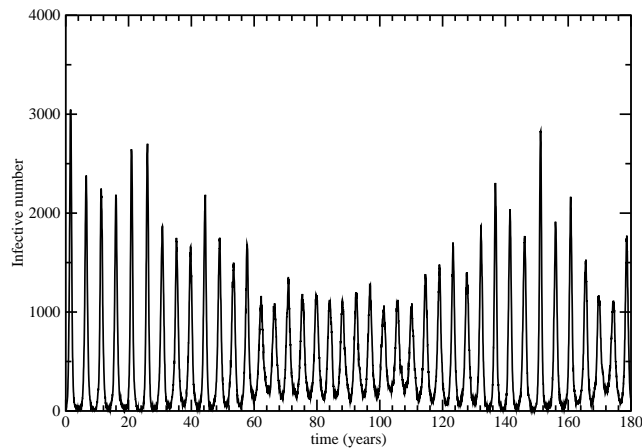
22

Figure 11.   Time series of the number of infectives for rubella, which has longer latency and infectious periods than measles and also lower infectiousness. Simulation in a 1000×1000 lattice with $p_{\mathrm{SW}} = 0.2$. The birth rate $\mu = 1/61$ yr^{-1} is the same as in the measles simulations, but now $\tau_{lat} = 12$ days, $\tau_{inf} = 12$ days and $\beta_0 = 1.32$ day^{-1}.

Our results suggest that measles is about three to four times more infectious then rubella and about twice as infectious as chickenpox. Given the crudeness of these estimations we can consider that the ratios agree quite well with those reported by Keeling & Grenfell [28]: 3.4 and 2.4 respectively for the transmissibility ratios and 2.5 and 1.4 for the effective transmission rate.[a] In another study [4] a value of 3.8 for the ratio of β_0's between measles and rubella was obtained by fitting the output of a seasonally forced SIR model to the data.

5. Discussion

The results in this paper show that both the short and long-term dynamics of childhood diseases conferring life-long immunity can be described by taking into account a dynamic small-world network of contacts. Moreover, the simulations make clear that the ability of recurrent epidemics to survive for a large number of cycles depends strongly on the level of heterogeneity

---

[a]Although their study focus on mumps instead of rubella, almost surely the two diseases have very similar values of infectiousness.
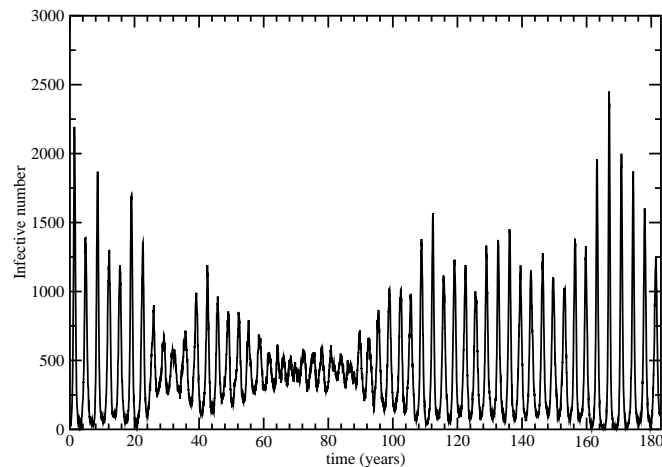
Figure 12.   Time series of the number of infectives for etiological parameters corresponding to chickenpox. Demographic parameters and small-world parameter are the same as for rubella and measles; $\tau_{lat} = 10$ days, $\tau_{inf} = 10$ days and $\beta_0 = 2.4$ day^{-1}.

in contact structure. The fraction of runs that survive up to a maximum ascribed time has a non-trivial dependence on the fraction of long-range contacts displaying, at low enough birth rates, a maximum at finite fraction of shortcuts. On the other hand, the persistence varies with the population size, and this gives the rationale on which to base a network-dependent Critical Community Size. The oscillations get more synchronized and their amplitude is strongly enhanced when p_{SW} is decreased below 1, *i.e.* as the weight of local contacts is increased. The amplitude cannot keep growing because the troughs between epidemic surges will get so deep, the number of surviving infectives so close to zero, that a stochastic fluctuation will eventually drive the epidemic extinct. This explains why an increase in amplitude is correlated with a decrease in persistence.

The small-world network allows us to go step by step from a dynamical system with a large number of degrees of freedom – which for $p_{SW} = 0$ are the $3N$ possible states of the lattice – to the case where the evolution can be captured by only a couple of ordinary differential equations. How this this contraction of phase space happens is an important but difficult question that deserves further investigation. We do know, however, the properties of the flow of the low dimensional deterministic system, namely that for the SIR ODE's the only attractor is a fixed point (s_0, i_0) and that there

24

is a saddle point at $(1,0)$ with its stable manifold along the $i_0 = 0$ axis. The fraction of infectives in the endemic steady-state is proportional to the birth rate, $i_0 = \mu(R_0 - 1)/\beta$, therefore as $\mu \to 0$, i_0 gets asymptotically close to the stable manifold. Since the real part of the pair of complex conjugate eigenvalues vanishes at zero birth rates one observes the critical slowing down of the dynamics at $\mu \to 0$. Small disturbances such as those provided by the stochastic drive will enable the system to make a large excursion in phase space before returning again to the vicinity of (s_0, i_0) where it is never allowed to settle.

It is clear that the progressive introduction of spatial degrees of freedom brings spatio-temporal coherence into the stochastic dynamics. The oscillations at small p_{SW} display a strong contribution from higher-order harmonics indicating that the system visits orbits located further away from the fixed point. Also, both the amplitude and period are larger than at larger values of p_{SW}, the oscillations evolving on a slower time scale compared to the less structured ones observed in the limit of random mixing. Clustering lowers the effective transmission rate and the average infective number but has the collateral effect of deepening the troughs and rising the peaks of oscillations. In the epidemic lows, infectives and susceptibles keep close together and the epidemic almost dies out. But one shortcut that randomly links an infective to the middle of a susceptible cluster will be enough to cause a large outbreak that may even consume every susceptible in that cluster. However some susceptibles will still remain in small clusters scattered all over the lattice and, screened from infection, their numbers will steadily grow at the (slow) pace dictated by the birth rate. Eventually one or more of these clusters will reach a size large enough that there will be a high probability of a long-range infection event linking to an individual inside them. When this happens the conditions are set for the cycle to repeat itself. When the fraction of shortcuts is high, susceptibles are steadily consumed at an intermediate rate and do not have time to aggregate into medium-size clusters. On the average the infection does spread more effectively – the average infective number is higher – but the large outbreaks are suppressed and what we observe instead are small, rapid fluctuations around an endemic state.

The simple fact that the PCA implementation of SIR and SEIR dynamics leads to sustained, fully developed oscillations as a consequence of heterogeneity in the network of contacts is by far the most impressive difference between our results and the output of deterministic mean-field models. However there are quantitative differences arising in quantities

that are very relevant for epidemiologists. The effective transmission rate β_{eff} is always smaller than the mean-field value β_0. In this respect our long-term simulations corroborate the results obtained from the simulation of a single epidemic outbreak [17]. R_0 is also lower than in the limit of random mixing. Moreover, in structured populations it is very important to distinguish between measurements of R_0 obtained from long time series and those focusing on a single outbreak because these two methods were shown to present the greater differences.

The SIR implementation can be used to access the qualitative impact of the network structure but to make the predictions of the PCA quantitative SEIR dynamics is required. Long time series, more than twice the length of the best available records can be easily obtained for realistic values of the model parameters and show a good agreement with observed values of the period and basic reproductive rate for measles and chickenpox. For rubella the agreement was only reasonable. In all the three cases the average age at infection is systematically underestimated, the discrepancy reaching 30 % in the case of rubella. The values obtained could be improved by accounting for immunity by maternal antibodies but still with this respect the PCA behaves no better than the mean-field models.

Different childhood diseases evolve on social networks that are similarly organized, transmission occurring predominantly in schools and households with a few exceptions corresponding to the long-range contacts. The structure of the contact patterns is thus identical and so are the demographic parameters. A realistic network model of childhood diseases must be able to discriminate between different diseases, in terms of T, A and R_0, purely as a result of the different latency and infectious periods plus the transmissibility β_0. The PCA satisfies this requirement and yields a reasonable estimate for the infectiousness of each disease.

6. Conclusion

The individual-based network model presented in this paper combines local structure with casual, long-range links. The latter are shortcuts through which the disease can propagate into regions where susceptibles predominate. Correlations that build up in the system due to network structure cause deviations from mean-field behaviour, but in the relevant limits the mean-field results are restored. Surprisingly, we found that, when the long-term evolution is considered, even with a small fraction of shortcuts the mean-field relations between the average age at infection, the basic re-

26

productive rate and the average number of susceptibles still hold. This consistency may explain why, although based on a unrealistic description of human contacts, deterministic models featuring homogeneous mixing remained for so long the basic conceptual tool of theoretical epidemiology. Their flaws, particularly the inability to describe recurrent epidemics, were exposed in the present work, in the context of childhood diseases. These are highly infectious diseases for which it is not unreasonable to assume that anyone who engages in any basic form of social interaction is equally at risk. Thus, we have disclosed the weaknesses of mean-field models in the case where they are certainly the less severe. Simulation of individual-based stochastic models becomes imperative in order to capture the dynamical complexity of infections like HIV of Hepatitis that spread on networks characterized by an extreme heterogeneity, like the network of sexual partnerships or needle sharing by intravenous drug users.

Acknowledgments

References

1. Anderson and May (1991), Infectious Diseases of Humans, Oxford University Press, Oxford.
2. Earn, David J. D. *et al.* (2000), A Simple Model for Complex Dynamical Transitions in Epidemics, *Science* **287**, 667-670.
3. Greenman, Jon, Kamo, Masashi, and Boots, Mike (2004), External Forcing of Ecological and Epidemiological Systems: a Resonance Approach, *Physica* D **190**, 136-151.
4. Keeling, Matt J., Rohani, Pejman and Grenfell, Bryan T. (2001), Seasonally Forced Disease Dynamics Explored as Switching Between Attractors, *Physica* D, **148**, 317-335.
5. Olsen, L. F. and Schaffer, W. M. (1990), Chaos versus Noisy Periodicity: Alternative Hypothesis for Childhood Epidemics, *Science* **249**, 499-504.
6. Rohani, Pejman, Keeling, Matthew J. and Grenfell, Bryan T. (2002), The Interplay between Determinism and Stochasticity in Childhood Diseases, *The American Naturalist*, **159**, 469-481.
7. Blasius, Bernd, Huppert, Amit and Stone, Lewi (1999), Complex Dynamics and Phase Synchronization in Spatially Extended Ecological Systems, *Nature*, **399**, 354-359.
8. Bailey, Norman T. J. (1975), The Mathematical Theory of Infectious Diseases, Charles Griffin, London.

9. Lloyd, Alen L. and May, Robert M. (1996), Spatial Heterogeneity in Epidemic Models, *J. Theor. Biol.*, **179**, 1-11.

10. Bolker, Benjamin and Grenfell, Bryan (1995), Space, Persistence and Dynamics of Measles Epidemics, *Phil. Trans. R. Soc. Lond.* B, **348**, 309-320.

11. Keeling, Matt J., Rohani, Pejman and Grenfell, Bryan T. (2000), Seasonally Forced Disease Dynamics Explored as Switching between Attractors, *Physica D*, **148**, 317-335.

12. Watts, D. J. and Strogatz, S. H. (1998), Collective Dynamics of 'Small-world' Networks, *Nature*, **393**, 440-442

13. Watts, D. J., Small Worlds (1999), Princeton University Press, Princeton, NJ.

14. Moore, Christopher and Newman, M. E. J. (2000), Epidemics and Percolation in Small-world Networks, *Physical Review* E, **61**, 5678-5682.

15. Newman, M. J., Jensen, I. and Ziff, R. M. (2002), Percolation and Epidemics in a Two-dimensional Small World, *Physical Review* E, **65**, 021904.

16. Boots, Michael and Sasaki, Akira (1999), "Small worlds" and the evolution of virulence: infection occurs locally and at a distance, *Proc. R. Soc. Lond.* B, **266**, 1933-1938.

17. Kleczkowski, A. and Grenfell, Bryan T., (1999), Mean-field-type equations for spread of epidemics: the "small world" model, *Physica A* **274**, 355-360.

18. Keeling, M. J. (1999), The effect of local spatial structure on epidemiological invasions, *Proc. R. Soc. Lond.* B, **266**, 859-867.

19. Johansen, Anders (1996), A Simple Model of Recurrent Epidemics, *J. Theor. Biol.*, **178**, 45-51.

20. Johansen, Anders (1994), Spatio-temporal Self-organization in a Model of Disease Spreading, *Physica D* **78**, 186-193.

21. Kuperman, Marcelo and Abramson, Guillermo, Small World Effect in an Epidemiological Model, *Phys. Rev. Lett.*, **86**, 2909-2911.

22. He, David and Stone, Lewi (2003), Spatio-temporal synchronization of recurrent epidemics, *Proc. R. Soc. Lond.* B, **270**, 1519-1526.

23. Verdasca, J. *et al.* (2005), Recurrent epidemics in small world networks, *J. Theor. Biol.*, **233**, 553-561.

24. Lloyd, Alun L. (2001), Realistic Distribution of Infectious Periods in Epidemic Models: Changing Patterns of Persistence and Dynamics, *Theor. Pop. Biol.*, **60**, 59-71.

25. Riley, S. R. et al., Transmission Dynamics of the Etiological Agent of SARS in Hong Kong: Impact of Public Health Interventions, *Science* **300**, 1961-1966.

26. Lipsitch, M. et al., Transmission Dynamics and Control of Severe Acute Respiratory Syndrome, *Science* **300**, 1966-1970

27. Diekmann O. and Heesterbeek, J. A. P. (2000), Mathematical Epidemiology of Infectious Diseases, Wiley, New York.

28. Keeling, Matt J. and Grenfell, Bryan T. (2000), Individual-based Perspectives on R_0, *J. theor. Biol.*, **203**, 51-61.